Method to traceably determine the refractive index by measuring the angle of minimum deviation

Martine Kuiper[1,2,3,4,*] ⓘ**, Richard Koops**[1]**, Rienk Nieuwland**[2,3] ⓘ
and Edwin van der Pol[2,3,4,5,6] ⓘ

[1] VSL, National Metrology Institute, Delft, The Netherlands
[2] Laboratory Experimental Clinical Chemistry, Amsterdam University Medical Centers, Location AMC, University of Amsterdam, Amsterdam, The Netherlands
[3] Vesicle Observation Center, Amsterdam University Medical Centers, Location AMC, University of Amsterdam, Amsterdam, The Netherlands
[4] Biomedical Engineering and Physics, Amsterdam University Medical Centers, Location AMC, University of Amsterdam, Amsterdam, The Netherlands
[5] Amsterdam Cardiovascular Sciences, Atherosclerosis and Ischemic Syndromes, Amsterdam, The Netherlands
[6] Cancer Center Amsterdam, Imaging and Biomarkers, Amsterdam, The Netherlands

E-mail: mkuiper@vsl.nl

CrossMark

Abstract

The refractive index (RI) of a solid depends on the illumination wavelength, temperature and material properties, such as the chemical composition, crystal structure, and isotropy. RI measurements, however, also depend on environmental conditions, such as the temperature, pressure, CO_2 concentration and humidity of the surrounding air. As these environmental conditions are not always reported, reported values of the RI are often irreproducible. Here we describe a new optical set-up based on the angle of minimum deviation to traceably measure the RI at controlled temperature, pressure, humidity, and CO_2 concentration of the surrounding air. Advantages of the reported method are that (I) we perform RI measurements without the need for an independent measurement of the prism angles, and (II) correlations in the uncertainty propagation reduce the sensitivity coefficients greatly. The absolute RI of fused silica at 20.00 °C is 1.470 091 at 404.66 nm, 1.467 169 at 435.83 nm, 1.460 459 at 546.07 nm, and 1.459 237 at 579.07 nm. The expanded uncertainty ($k = 2$) of the set-up and procedure is 1.4×10^{-6} for 404.66 nm, 435.83 nm, and 546.07 nm and 1.7×10^{-6} for 579.07 nm. The main factors affecting the expanded uncertainty are the calibration uncertainty of the rotary stage, and the repeatability of the measurement.

Keywords: angle of minimum deviation, fused silica, measurement uncertainty, standardization, refractive index, traceable measurements, uncertainty budget

S Supplementary material for this article is available online

(Some figures may appear in colour only in the online journal)

1. Introduction

The refractive index (RI) of a solid depends on the illumination wavelength, temperature and material properties, such as the chemical composition, crystal structure, and isotropy. The RI can therefore be used as a quality control for the fabrication of lenses [1], mirrors [2], prisms [3–6], optical fibres [1], and to identify biological particles [7]. However, literature values of the measured RI of the same material show variation. For example, figure 1(a) shows the RI of fused silica reported at a wavelength of 546 nm by 12 different studies, resulting in a variation of 0.000 771 in the RI of fused silica, and figure 1(b) shows the variations in the reported RI of fused silica over several wavelengths reported by 21 different studies. In figure 1(b), the maximum variation in the reported RI values of fused silica of 0.002 108 occurs at a wavelength of 589 nm. In figure 1, we related the reported RIs to the RI at 20 °C using the thermo-optic coefficient from either Leviton *et al* (2006) or the thermo-optic coefficient reported in the reference [3, 8–10].

The variation in reported RI values may be caused by differences in the reported type of RI (either absolute or relative to air), differences between materials properties, but also by differences in environmental conditions, such as the temperature, pressure, and humidity of the surrounding air. When performing RI measurements, the environmental conditions should be controlled and reported [11]. Additionally, also the fluctuations of the environmental conditions should be reported because these fluctuations determine the smallest uncertainty that can be achieved during the RI measurements. Especially the environmental temperature should be well controlled, because fluctuations of more than 0.167 °C lead to an uncertainty of 10^{-5} when using the minimum deviation method for glasses with a thermo-optic coefficient of 3×10^{-5} K [12], assuming that the glass is in thermodynamic equilibrium with the environment. Table 1 provides an overview of the reported environmental conditions, their fluctuations, and measurement uncertainties for the RI of fused silica. Table 1 shows that none of the 21 studies reported the measured RI type (absolute or relative to air), all relevant environmental conditions and/or their fluctuations. Consequently, the measurement uncertainties of the reported results in table 1 are probably underestimated and the measured RIs are not reproducible.

In this manuscript, we describe a new and traceable method to determine the absolute RI of a prism that is based on the minimum deviation method. Existing methods require separate prism angle measurements. Additionally, existing methods with similar measurement uncertainty require two measurements per prism angle as well as two measurements per minimum deviation angle [13]. Our new method simultaneously measures the RI and prism angles, thereby relinquishing the need for separate prism angle measurements. We report all relevant environmental conditions and their fluctuations at the time of measurement, describe the experimental set-up and identify each factor contributing to its uncertainty budget [14]. As all relevant external factors and their fluctuations are
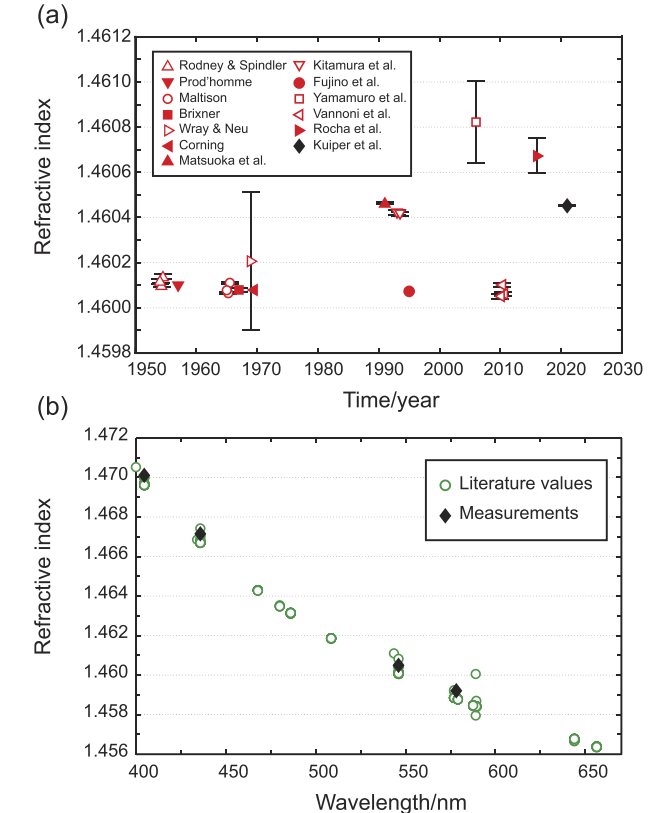

Figure 1. Comparison of the RI of fused silica found in literature and measured by the method described in this manuscript. (a) RI of fused silica found in literature (triangles, squares, circles) and measured by us (diamond) at a wavelength of 546 nm versus the time in years. For measurements in the same year, the time can have an offset of 0.25. The black error bars show the uncertainties mentioned for each of the measurements. (b) RI from the literature (circles) and our measurements (diamonds) at 20 °C versus wavelength. The RI decrease for increasing wavelengths.

determined and reported, the measured RI depends only on the material properties. We measure an equilateral fused silica prism with the new method and compare our results to those reported in literature. Ultimately, this method will be used for fast and accurate measurements of the RI of buffer fluids used in biomedical applications.

2. Method

2.1. Angle of minimum deviation

When a beam of light propagates through an interface between two materials of different RIs, the beam refracts. A beam propagating through a prism is refracted twice, as shown in figure 2. The angle between the incident and emerging beam is called the deviation angle. The deviation angle of a prism depends on the angle of incidence and reaches a minimum, θ_{MD}, if the angles of refraction at both interfaces are equal and if the angle of incidence, θ_a, and the angle of emergence are equal [30]. Based on Snell's law and goniometry, the absolute

Table 1. Environmental conditions reported for the RI of fused silica measured by different methods. Environmental conditions that are important to report are the temperature, pressure, humidity, and the fluctuations thereof. We assume that the glass is in thermodynamic equilibrium with the environment. In addition, the table shows the claimed uncertainty and type of fused silica measured[a].

Method	RI type	$T \pm \Delta T$/°C	$P \pm \Delta P$/hPa	$H \pm \Delta H$/RH%	Uncertainty	Fused silica type	References
—	—	—	—	—	—	C 7940	[15] [b]
—	—	—	—	—	—	C 7940	[2]
R	—	—	—	—	—	—	[16]
I	—	25	—	—	—	SRM-739	[17]
3P	—	20	—	—	—	—	[15] [b]
B	—	—	—	—	2×10^{-4}	Suprasil	[18]
M	—	23	—	—	—	C 7940	[19]
I	—	22	—	—	2×10^{-3}	Suprasil I	[15, 20]
B	—	25	—	—	1×10^{-3}	Vitreosil	[21, 22]
M	—	20	—	—	5×10^{-6} to 1×10^{-5}	C 7940/Dynasil/G.E. 151	[23]
M	—	20	—	—	9.3×10^{-6}	C 7940/Dynasil/G.E. 151	[24]
I	a	30	—	—	8×10^{-5}	Heraeus	[10]
M	a	21.85	—[c]	—	1×10^{-5}	C 7980	[8]
M	—	26[d]	—[c]	—	3.1×10^{-4}	C 7940	[3]
M	a	20.5	5×10^{-8}	—	3×10^{-6}	Type III Nippon Sekiei	[25]
I	—	20 ± 0.02	—	—	2×10^{-5}	C 7940	[26]
M	a	20.85 ± 2	—	—	1.8×10^{-4}	—	[27]
M	—	24 ± 0.2	—	45	1×10^{-5}	G.E./Heraeus/Nieder/C	[28]
M	a	25 ± 0.3	1000	—	1×10^{-5}	—	[9]
I	a	22 ± 0.5	1013.25 ± 20.27	—	2.7×10^{-5}	Esco optics	[1]
M	r	19.85 ± 1	1×10^{-4}	45 ± 5	1×10^{-5}	Lithosil/Suprasil 312	[29]

[a]RI: refractive index; T: temperature; ΔT: temperature fluctuation; P: atmospheric pressure; ΔP: pressure fluctuation; H: humidity; ΔH: humidity fluctuation; Ref.: reference; R: reflection; I: interferometry; 3P: three prisms method; B: Becke line; M: minimum deviation; a: absolute; r: relative; C: corning; G.E.: general electric.

[b]The original source was not available.

[c]In vacuum.

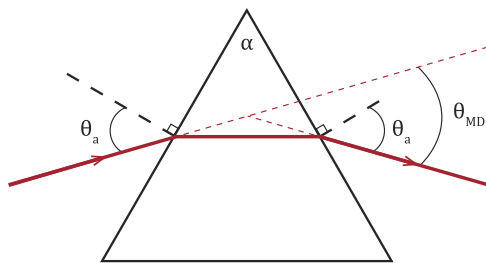[d]Has been accounted for in the uncertainty.

Figure 2. Angle of minimum deviation of a beam propagating through a prism. When a beam of light (solid red line) propagates through an interface between two materials of different RIs, the beam refracts. A beam propagating through a prism is refracted twice. The beam enters a prism with angle θ_a, the angle of incidence. The angle between the incidence and emerging beam is called the deviation angle. The smallest deviation angle is the angle of minimum deviation, θ_{MD}, which is reached when the angle of incidence and emergence are equal. To determine the RI of a prism, also the prism angle α is needed.

RI of a prism n_{prism} is related to the RI of air n_{air}, θ_a, the prism angle α, which is the angle between the two refracting faces of the prism [30], and θ_{MD} as follows:

$$n_{prism} = n_{air} \frac{\sin(\theta_a)}{\sin\left(\frac{\alpha}{2}\right)} = n_{air} \frac{\sin\left(\frac{\alpha + \theta_{MD}}{2}\right)}{\sin\left(\frac{\alpha}{2}\right)}. \tag{1}$$

Thus, when α and n_{air} are known, measurements of θ_{MD} can be used to determine n_{prism}. When α is unknown, with the prism 180 degrees rotated, a second measurement θ_{MD} in the other direction creates two independent measurements with two unknowns (α and n_{prism}).

2.2. Set-up

Figure 3 shows a schematic overview of the set-up. In the set-up, spectral lines from a mercury lamp (Pen-Ray, Ultra Violet Products, Inc., San Gabriel, CA, USA) were spectrally filtered (#65-072 (405 nm), #65-077 (436 nm), #65-097 (546 nm), #65-100 (580 nm), Edmund Optics, Barrington, NJ, USA) to select the wavelengths 404.66 nm, 435.83 nm, 546.07 nm, and 579.07 nm. The spectral filters were mounted on a motorized filter wheel (Ell9, Thorlabs, Newton, NJ, USA) to allow automated selection. Filtered light passed through a 200 μm slit and was collimated by a positive achromatic doublet lens with a focal length of 200 mm (AC508-200 A, Thorlabs, Newton, NJ, USA) before passing through a S1-UV fused silica equilateral prism (Esco Optics, Oak Ridge, NJ, USA). The prism was mounted on a motorized rotary table (UPR-270-AIR, PI-Micos, Karlsruhe, Germany). After passing the prism, the light was focussed on a camera (DCC1545M-GL, Thorlabs, Newton, NJ, USA) using a singlet lens with a focal length of 200 mm (LA1708-A-ML, Thorlabs, Newton, NJ, USA). The camera settings were adjusted to prevent saturation
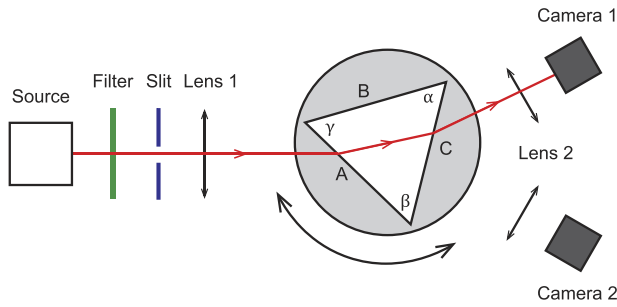
Figure 3. Schematic overview of the RI measurement set-up. The set-up with from left to right the illumination source, filter, slit, collimating lens, rotary table with the equilateral prism on top, focussing lenses and cameras. Spectral lines from a mercury source are filtered (green line) to select wavelengths 404.66 nm, 435.83 nm, 546.07 nm, and 579.07 nm. Filtered light passes through a 200 μm slit (blue line) and is collimated by a positive achromatic doublet lens, lens 1, with a focal length of 200 mm before passing through a fused silica prism mounted on a rotary table (grey circle). After passing the prism, the light is focussed on a camera using a positive singlet lens, lens 2, with a focal length of 200 mm.

of the sensor. The pixel clock was set to 20 MHz, the frame rate was set to 10 fps and the exposure time was set between 50 and 80 ms depending on the ambient light.

With the set-up, an image of the slit onto the camera was created. The image position was proportional to the angle of the emerging beam. To measure the angles of minimum deviation, the rotary table was rotated over either 2.5 degrees with an interval of 0.05 degrees (404.66 nm, 435.83 nm, and 546.07 nm) or 10 degrees with an interval of 0.5 degrees (579.07 nm). Supplementary 1 shows an additional picture of the set-up as described in figure 3.

2.3. Procedure

To determine n_{prism} from measurements of θ_{MD}, but without prior knowledge of the prism angles $\alpha \cdot \gamma$, two measurements of θ_{MD} were performed by two cameras at each prism face $A \cdot C$ of a near-equilateral prism, resulting in six consecutive measurements of θ_{MD}. We started the measurement series with face A perpendicular to the incoming beam. The angle which the rotary table documents at this starting position, θ_0, is the origin angle of the rotary table in degrees. The measurements of the angles generated by the rotary table are traceable to SI units.

We started with measuring angle θ_{AC}, one of the six angles measured with the calibrated rotary table at θ_{MD}, where the subscript AC denotes the faces A and C where the beam is propagating through, as shown in figure 3. For the first three measurements, which correspond to measuring the angles θ_{AC}, θ_{BA}, and θ_{CB}, the prism was rotated counter clockwise in negative direction and camera 1 was used. For the last three measurements, which correspond to measuring the angles θ_{CA}, θ_{BC}, and θ_{AB}, the prism was rotated clockwise in positive direction and camera 2 was used. The direction of the rotation was kept constant for measurements on the same camera to avoid backlash of the rotary table. The equations for the six measurements are given by:

$$\theta_{AC} = \theta_0 - \theta_b \tag{2}$$

$$\theta_{BA} = \theta_0 - \theta_c - (180° - \gamma) \tag{3}$$

$$\theta_{CB} = \theta_0 - \theta_a - (180° - \gamma) - (180° - \alpha) \tag{4}$$

$$\theta_{CA} = \theta_0 + \theta_b - (180° - \gamma) - (180° - \alpha) \tag{5}$$

$$\theta_{BC} = \theta_0 + \theta_a - (180° - \gamma) \tag{6}$$

$$\theta_{AB} = \theta_0 + \theta_c \tag{7}$$

where $\theta_a \cdot \theta_c$ are the angles of incidence (and emergence) for θ_{MD} of each prism angle in degrees. Supplementary 2 contains a figure with all the angles from measurements as mentioned in equations (2)–(7), as well as the matrix inversion to derive equations (8)–(13) from equations (2)–(7).

Next, the following set of linear equations (2)–(7) were solved for $\alpha \cdot \gamma$ and $\theta_a \cdot \theta_c$:

$$\alpha = 180° - ((\theta_{BA} + \theta_{AB}) - (\theta_{AC} + \theta_{CA})) \tag{8}$$

$$\beta = -180° - ((\theta_{CB} + \theta_{BC}) - (\theta_{BA} + \theta_{AB})) \tag{9}$$

$$\gamma = 180° - ((\theta_{AC} + \theta_{CA}) - (\theta_{CB} + \theta_{BC})) \tag{10}$$

$$\theta_a = \frac{1}{2}((\theta_{BC} - \theta_{CB}) - (180° - \alpha)) \tag{11}$$

$$\theta_b = \frac{1}{2}((\theta_{CA} - \theta_{AC}) + (180° - \gamma) + (180° - \alpha)) \tag{12}$$

$$\theta_c = \frac{1}{2}((\theta_{AB} - \theta_{BA}) - (180° - \gamma)) \tag{13}$$

where we used the additional constraint that the sum of the prism angles $\alpha \cdot \gamma$ is exactly 180°. Consequently, this method allowed simultaneous determination of θ_{MD} and the prism angles, thereby eliminating the uncertainty associated with a separate prism angle measurement. Next, equation (1) was solved for α and θ_a, β and θ_b, and γ and θ_c, providing three values for RI. For the determination of the RI of the prism, the mean was taken of the three individual determinations of the RI.

2.4. Environmental conditions

The set-up was located in a level 7 cleanroom with controllable environmental conditions. The environmental conditions are traceable to SI through the respective national standards. During the measurements the environmental conditions were as follows. The temperature at the sample was $(20.00 \pm 0.03)\,°C$, the atmospheric pressure was (1011.4 ± 0.4) hPa, the humidity was (45.8 ± 0.4) %RH, and the CO_2 concentration was (450 ± 100) ppm. The temperature affects the RI of air and the RI of the prism. In addition, the atmospheric pressure, humidity, and CO_2 concentration affect the RI of air and therefore were logged during the RI measurements. Fluctuations in temperature, atmospheric pressure and humidity were within the values from ISO 21395-1:2020 for RI measurements of optical glasses for our reported uncertainty, because fluctuations determine the best uncertainty which can be obtained
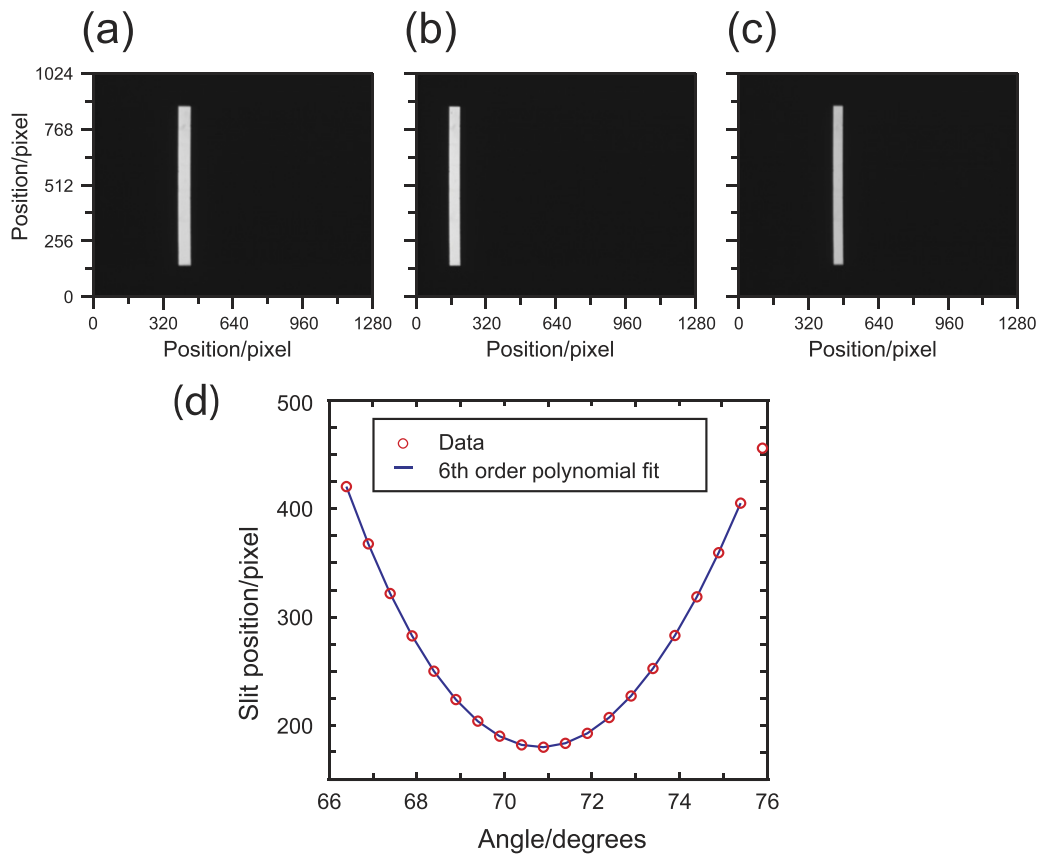
Figure 4. Measurement of the angle of minimum deviation at a wavelength of 546 nm. (a) Light passing through the 200 μm slit imaged on the camera for an angle smaller than the angle of minimum deviation (data point 1 in panel (d)). (b) When the image of the slit is at the angle of minimum deviation, the imaged slit is at the uttermost left point (data point 10 in panel (d)). (c) Increasing the angle makes the slit move to the opposite side of the camera (datapoint 20 in panel (d)). (d) Measured (symbols) peak position of the imaged slit versus angle fitted by a 6th order polynomial (line). The minimum corresponds to the angle of the rotary table at the angle of minimum deviation. The vertical axis displays the pixel number of the slit position as seen in panels (a)–(c). Measured peak positions not connected to the polynomial fit are removed by forced symmetry to improve polynomial fit accuracy, as the polynomial fit works most accurate for a balanced data set.

[12]. This ISO guideline does not provide guidelines for fluctuations in the CO_2 concentration, because the effect of the CO_2 concentration on the RI of air is in the range of 10^{-8}.

2.5. Data analysis

Each measurement generated 20 data points of the angle of the rotary table and 20 images of the corresponding slit position. With each angle of the rotary table, the position of the slit on the camera image changed, and at the angle of minimum deviation the slit was either at the most left (camera 2) or right position (camera 1). Figure 4 shows an example of the change in the position of the slit on the camera for fused silica measured at a wavelength of 546.07 nm. Figure 4(a) shows the first measurement of the slit position, figure 4(b) shows the position of the slit at the angle of minimum deviation, and figure 4(c) shows the last measurement of the slit position, where the slit position on the camera is going back towards the centre of the camera. From figures 4(a)–(c) we get the data of the slit position from central pixel of the slit.

Figure 4(d) shows the slit position versus the measured angle of the rotary table. To find the position of the slit at the angle of minimum deviation, the data were fitted with a sixth order polynomial fit [31]. The minima (camera 2) or

maxima (camera 1) of the fits corresponded to the angles of the rotary table at the angles of minimum deviation, $\theta_{AC} \cdot \theta_{AB}$ in equations (2)–(7). Using the ray tracing model discussed in the next paragraph, we verified that for a 10 degree range, a sixth order polynomial was sufficiently accurate to fit the data to the non-linear curve representing the relation between rotation angle and deviation angle.

2.6. Ray tracing model

To determine the contribution of sources of uncertainty to the expanded uncertainty of the measured RI, we performed Monte Carlo simulations of a ray tracing model in MATLAB (version 2010b, MathWorks, USA) [32]. The ray tracing model used Snell's law and the input parameters for the sources of uncertainty to determine the path of the ray through the prism for all six measurements to determine the RI of the prism. To obtain the probability distribution of the complete RI measurement, the Monte Carlo simulations trace random rays based on the probability distributions of seven sources of uncertainty. These sources of uncertainty were the (i) RI of air, (ii) calibration of the rotary table, (iii) effect of wavelength on the RI due to the dispersion of fused silica, (iv) effect of the temperature of the prism, (v) flatness of all three faces
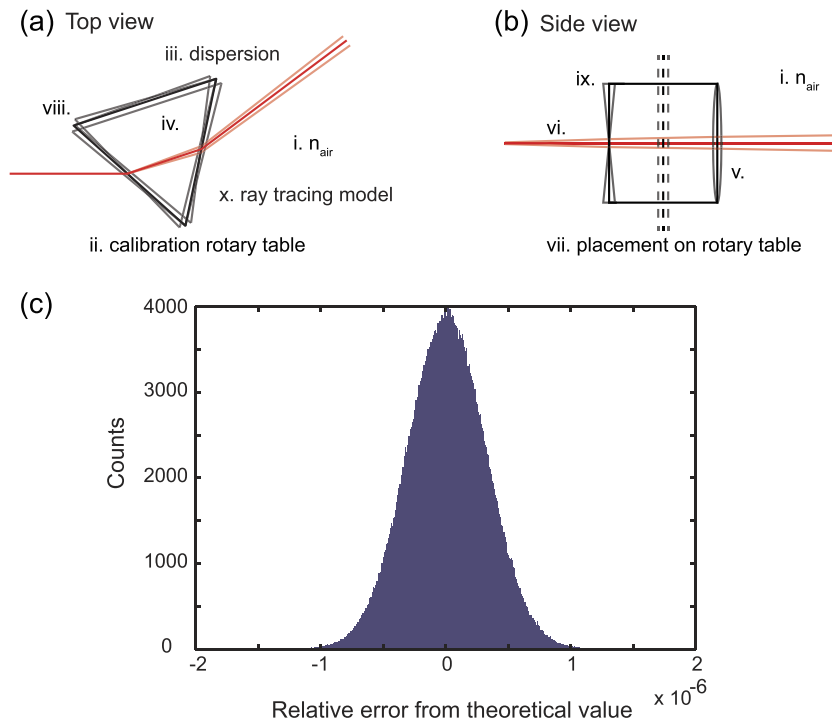
Figure 5. The sources of uncertainty affecting RI measurements of the prism according to the ray tracing model viewed from (a) the top and (b) the side. Sources of uncertainty being calculated in the model are the (i) RI of air, (ii) calibration of the rotary table, (iii) effect of dispersion, (iv) effect of prism temperature, (v) flatness of all three faces (of incidence and emergence), (vi) vertical alignment of the light source relative to the rotary table, (vii) placement of the prism on the rotary table, (viii) deviation of the prism angles from equilateral, (ix) deviation of the pyramid angles from perpendicular to the prism base, and (x) ray tracing model itself. (c) Monte Carlo simulation (number of simulations: 10^6) of the uncertainty sources of the experimental set-up during a fused silica measurement at a wavelength of 546 nm. The histogram shows a normal distribution with a standard deviation representing the standard uncertainty. The standard uncertainty without considering the repeatability is 3.5×10^{-7}.

(of incidence and emergence), (vi) vertical alignment of the light source relative to the rotary table, (vii) placement of the prism on the rotary table, (viii) deviation of the prism angles from equilateral, (ix) deviation of the pyramid angles from perpendicular to the prism base, and (x) uncertainty from the model using a sixth order polynomial. To indicate the sources of uncertainty, figures 5(a) and (b) show a top view and side view of the prism, respectively.

Each of the sources of uncertainty was quantified to determine their contribution to the expanded uncertainty. The uncertainty in the RI of air was 1.149×10^{-7}. This value is based on the Edlén equation [33] with the measured environmental conditions and their fluctuations during the measurement, and the wavelength of the spectral lines and uncertainty in this wavelength as input parameters. The uncertainty for the rotary table calibration was $\sqrt{\left(\left(\frac{0.4}{2}\right)^2 + 0.2^2\right)}$ arcsecond, based on the rotary table calibration. The calibration of the rotary table was performed with a 36-sided polygon and two calibrated autocollimators using a full circle closure measurement. This resulted in both the calibration of the polygon itself and the errors of the table at 36 angle positions. The expanded uncertainty of the rotary table calibration was 0.4 arcsecond. The errors of the table were subsequently corrected, leaving a residue of the error of 0.2 arcsecond. Additionally, the uncertainty in the wavelength of the spectral lines was 1×10^{-4} nm [34].

The effect of the uncertainty in wavelength on the RI of silica due to the dispersion of fused silica was calculated using the dispersion relation from Malitson *et al* at 405 nm, where we calculated $\frac{dn}{d\lambda} = -0.10495 \ \mu m^{-1}$, which yields d$n = 1.0 \times 10^{-8}$ [23]. The uncertainty contribution due to the fluctuations in the temperature of the fused silica prism was determined by multiplying the thermo-optic coefficient from Leviton [8] and the fluctuation of the temperature during the measurement. The uncertainty due to the flatness deviation of the prism faces was 0.00115 degrees, based on the maximum flatness deviation of 400 nm measured by Fizeau interferometry divided over 20 mm of the surface. The uncertainty for the vertical alignment of the light source relative to the rotary table was atan$\left(\frac{0.1}{500}\right)$, based on the maximum input error of the slit position (0.1 mm) and the distance between the slit and the camera (500 mm). The uncertainty for the prism placement on the rotary table took into account a misalignment of 0.8 mm between the centre of mass of the prism and the centre of the rotary table. The deviation of the prism angles from $60°$ were 0.03431, 0 and -0.030252 degrees, and the deviation of pyramid angles from $90°$ were 0.0019, 0.0016 and 0 degrees. Lastly, the uncertainty contribution of the ray tracing model itself using a sixth order polynomial was determined with all other uncertainty sources set to zero.

To determine the angle of minimum deviation, the ray tracing model used the angle of emergence, which equivalent

to imaging the position of the slit onto a camera. The number of runs of the Monte Carlo simulation was 10^6, which was sufficient to find reliable uncertainties according to ISO 98-3:2008 [35].

3. Results

3.1. RI measurements

Table 2 shows the measured RI of the fused silica prism at 20.00 °C for wavelengths of 404.66 nm, 435.83 nm, 546.07 nm, and 579.07 nm. Figure 1(a) shows the measured RI of fused silica at 546 nm wavelength compared to values reported in the literature versus the time in years. When reported (see table 1), the uncertainties are indicated by error bars. Our RI estimate of fused silica at 546 nm wavelength lies within the range of literature values, but in general the reported RIs differ from each other and are not consistent within the uncertainties.

Table 2. RI measurements of fused silica at four wavelengths at 20.00 °C at an expanded uncertainty of 1.4×10^{-6} (404.66 nm, 435.83 nm and 546.07 nm) and a slightly higher expanded uncertainty for 579.07 nm of 1.7×10^{-6} due to a range of rotation of 10 degrees and an interval of 0.5 degrees.

Wavelength/nm	RI
404.66	1.470 091
435.83	1.467 169
546.07	1.460 459
579.07	1.459 237

Figure 1(b) shows the RI measurements and literature values of fused silica (reported by all 21 different studies in table 1) versus wavelength. For each wavelength, there is a range of RIs and our data fall within this range for each of the wavelengths. The reported uncertainties are not shown but can be found in table 1.

3.2. Uncertainty

Using Monte Carlo simulations of a ray tracing model, the contribution of sources of uncertainty to the expanded uncertainty were determined. The individual contribution for each uncertainty source was evaluated with the model by using only the corresponding uncertainty contribution and setting all others to zero. Figure 5(c) shows the probability distribution of the relative expanded uncertainty of the RI measurement, as determined by the Monte Carlo simulations. The contribution of each source of uncertainty to the expanded uncertainty was calculated from the histogram by using the mean error, and the standard deviation using the offset and width of the histogram.

Due to specific correlations in the uncertainty propagation in our procedure, the sensitivity coefficients of sources of uncertainty are greatly reduced. For example, for the air RI, since

$$n_{\text{prism}} = n_{\text{air}} \times n_{\text{rel}} \tag{14}$$

where n_{rel} is the relative RI between n_{prism} and n_{air}, the sensitivity coefficient is calculated via

$$\frac{\delta n_{\text{prism}}}{\delta n_{\text{air}}} = n_{\text{rel}} + n_{\text{air}} \times \frac{\delta n_{\text{rel}}}{\delta n_{\text{air}}} \tag{15}$$

where $\frac{\delta n_{\text{rel}}}{\delta n_{\text{air}}}$ is the partial derivative from n_{rel} with regards to n_{air}. The second term arises because the calculation of n_{rel} also involves n_{air}. In our case, the magnitude of the second term is almost equal to the first term but of opposite sign, since according to our Monte Carlo model the partial derivative turns out to be negative. The resulting sensitivity coefficient, see table 3, is therefore orders of magnitude smaller compared to the conventional result assuming that n_{rel} is independent of n_{air}.

Table 3 shows the uncertainty budget of the RI measurements, which contains the sources of uncertainty calculated with the Monte Carlo method and the repeatability of the RI measurement. The repeatability accounts for the variability in measurements under repeatable conditions and was determined by performing 20 consecutive measurements at 405 nm and at controlled environmental conditions. The uncertainty due to the repeatability was calculated by taking the standard deviation of the average RI of all measurements, divided by the root of the number of measurements. Table 3 shows that the largest sources of uncertainty are repeatability, and calibration of the rotary table. The deviation of the prism angles from equilateral has no effect on the expanded uncertainty. The expanded uncertainty of the set-up is 1.4×10^{-6} with a coverage factor of $k = 2$, indicating a 95% confidence interval.

4. Discussion

The experimental set-up and method described in this manuscript can simultaneously measure the RI and prism angles of a fused silica prism. We compared our RI measurement of a fused silica prima to those reported in the literature. Figure 1 shows a wide range of RI values reported for fused silica, which can result from differences in material properties and/or in environmental conditions. The literature values are difficult to interpret, however, due to incomplete reporting of the environmental conditions (see table 1). Therefore, it is difficult to conclude whether the observed variation in the reported RI values results from absolute measurements or measurements relative to air, differences in material properties and/or environmental conditions. The reported RIs and uncertainties presented in the present manuscript only depend on the material properties, because all relevant environmental conditions are controlled, measured and taken into account in the uncertainty budget.

Compared to earlier minimum deviation methods, our set-up has two limitations and four advantages. The first limitation is that in the automated form, the prism angles have to be close to 60 degrees, because otherwise the cameras have to be moved between subsequent measurements, which would substantially increase the measurement time. Secondly, we perform not one but six measurements of the angle of minimum deviation.

Table 3. Uncertainty budget for the RI of fused silica at 404.66 nm at 20.00 °C[a].

Source of uncertainty	Standard uncertainty	Unit	Distribution	Sensitivity coefficient	Unit	Uncertainty contribution
Repeatability ($n = 20$)	5.9×10^{-7}		Normal	1.0		5.9×10^{-7}
Air RI	1.2×10^{-7}		Normal	6.9×10^{-4}		7.9×10^{-11}
Calibration of the rotary table	7.9×10^{-5}	°	Normal	4.8×10^{-3}	/°	3.8×10^{-7}
Effect dispersion	1.0×10^{-8}		Normal	1.0		1.0×10^{-8}
Effect prism temperature	9.7×10^{-8}		Rectangular	1.0		9.7×10^{-8}
Flatness of the faces	6.6×10^{-4}	°	Rectangular	1.2×10^{-7}	/°	7.9×10^{-11}
Input beam alignment	1.1×10^{-2}	°	Rectangular	5.7×10^{-7}	/°	6.3×10^{-9}
Placement of the prism on the rotary table	2.9×10^{-1}	mm	Rectangular	2.7×10^{-10}	/mm	7.9×10^{-11}
Prism angle	3.4×10^{-2}	°	Rectangular	2.2×10^{-9}	/°	7.6×10^{-11}
Pyramid angle	1.1×10^{-3}	°	Rectangular	2.4×10^{-7}	/°	2.7×10^{-10}
Ray tracing model	7.6×10^{-11}		Normal	1.0		7.6×10^{-11}
Combined standard uncertainty						0.7×10^{-6}
Expanded uncertainty ($k = 2$)						1.4×10^{-6}

[a]*n*: number of measurements; *k*: coverage factor.

However, this limitation is overcome by automation of the experimental set-up.

The main advantage is that the set-up measures the RI and prism angles simultaneously. Consequently, the prism angles do not need to be measured by a separate method, and therefore our method is fast and easy to use, and there are no additional contributions to the uncertainty budget due to prism angle measurements. A second advantage is the use of cameras to measure the angle of minimum deviation, because the images provide information about prism angles and pyramid angles of the prism. Third, this set-up does not use mirrors, thereby avoiding an extra source of uncertainty. Fourth, the correlations in the measurement procedure ensure reduced sensitivity coefficients in a number of sources of uncertainty such as the air RI, therefore reducing the overall measurement uncertainty.

The experimental set-up has an expanded uncertainty of 1.4×10^{-6}, which meets our target expanded uncertainty of 10^{-5}. The next step is to replace the solid prism with a prism containing a fluid cell and perform RI measurements of fluids. To investigate if new sources of uncertainty affect the expanded uncertainty, we performed simulations of the experimental set-up combined with a fluid cell. New sources of uncertainty added to the simulated include the parallelism of the windows as stated by the manufacturer (input value: 30 arcseconds), and the uncertainty in the RI of the windows taken from literature (input value: 0.1). All sources of uncertainty contributed below 10^{-7} towards the expanded uncertainty, meaning that the new sources are not expected to affect the expanded uncertainty of the set-up with a fluid cell. Thus, the solid prism and prism containing a fluid cell are expected to yield the same expanded uncertainty, and the set-up is ready to perform measurements on fluids for nanoparticle research.

One application of the set-up with a fluid cell is to obtain the RI of buffer fluids used in extracellular vesicle (EV) research. EVs are cell-derived (biological) particles present in all body fluids and can be used as biomarkers for health and disease.

A commonly used technique to measure EVs is flow cytometry, which is a laser-based technique which measures light scattering signals and fluorescence from single EVs in buffer fluids. To standardize EV measurements with flow cytometry, the light scattering signals are related to the diameter of EVs by Mie theory [36]. To allow traceable sizing, both the effective RI of the EVs and the RI of the buffer fluid must be known. As part of the METVES II project, we will measure the RI of typical buffer fluids using the set-up described in this manuscript.

5. Conclusion

We developed a measurement method to simultaneously determine the RI and prism angles of a solid prism. We validated the experimental set-up performance with Monte Carlo simulations of a ray tracing model to establish the measurement uncertainty. The method was applied to measure the RI and prism angles for a fused silica prism at wavelengths 404.66 nm, 435.83 nm, 546.07 nm, and 579.07 nm. The RI can be determined with an expanded uncertainty of 1.4×10^{-6} ($k = 2$). Addition of a fluid cell does not affect the expanded uncertainty, as new sources of uncertainty do not increase the expanded uncertainty. Therefore, the set-up is ready to perform measurements of buffer fluids, for example as used in EV research.

Acknowledgments

ORCID iDs

Martine Kuiper ⬭ https://orcid.org/0000-0002-4533-8617
Rienk Nieuwland ⬭ https://orcid.org/0000-0002-5394-2152
Edwin van der Pol ⬭ https://orcid.org/0000-0002-9497-8426

References

[1] Lee C, Choi H, Jin J and Cha M 2016 Measurement of refractive index dispersion of a fused silica plate using Fabry–Perot interference *Appl. Opt.* **55** 6285–91

[2] Rathmann C L, Mann G H and Nordberg M E 1968 A new ultralow-expansion, modified fused-silica glass *Appl. Opt.* **7** 819–23

[3] Wray J H and Neu J T 1969 Refractive index of several glasses as a function of wavelength and temperature *J. Opt. Soc. Am.* **59** 774–6

[4] Hirai A, Hori Y, Minoshima K, Pisani M and Astrua M 2012 A bilateral comparison of optical glass refractive index between NMIJ and INRiM for the validation of the measuring systems *Metrologia* **49** 283

[5] Hori Y, Hirai A and Minoshima K 2011 Prism-pair interferometry by homodyne interferometers with a common light source for high-accuracy measurement of the absolute refractive index of glasses *Appl. Opt.* **50** 1190–6

[6] Astrua M and Pisani M 2009 Prism refractive index measurement at INRiM *Meas. Sci. Technol.* **20** 095305

[7] Kuiper M, van de Nes A, Nieuwland R, Varga Z and van der Pol E 2021 Reliable measurements of extracellular vesicles by clinical flow cytometry *Am. J. Reprod. Immunol.* **85** e13350

[8] Leviton D B and Frey B J 2006 Temperature-dependent absolute refractive index measurements of synthetic fused silica *Optomechanical Technologies for Astronomy* (International Society for Optics and Photonics vol 6273) p 62732K

[9] Kitamura N, Toguchi Y, Funo S, Yamashita H and Kinoshita M 1993 Refractive index of densified silica glass *J. Non-Cryst. Solids* **159** 241–5

[10] Rocha A C P, Silva J R, Lima S M, Nunes L A O and Andrade L H C 2016 Measurements of refractive indices and thermo-optical coefficients using a white-light Michelson interferometer *Appl. Opt.* **55** 6639–43

[11] Tilton L W 1929 Prism Refractometry and Certain Goniometrical Requirements for Precision *J. Res. of NBS* **2** 909–30

[12] International Organization for Standardization 2020 *Optics and Photonics—Test Method for Refractive Index of Optical Glasses: I. Minimum Deviation Method*

[13] Vishnyakov G N, Fricke A, Parkhomenko N M, Hori Y and Pisani M 2016 Report on supplementary comparison COOMET.PR-S3: refractive index *Metrologia* **53** 2001

[14] Tentori-Santa-Cruz D and Lerma J R 1990 Refractometry by minimum deviation: accuracy analysis *Opt. Eng.* **29** 160–8

[15] Mazurin O V, Streltsina M V and Shvaiko-Shvaikovskaya T P 2012 *Silica Glass and Binary Silicate Glasses* (Amsterdam: Elsevier)

[16] Venediktov A A, Morozov V N and Polukhin V N 1969 Reflection spectra of crystalline and vitreous modifications of GeO_2 and SiO_2 in the (5–50) μ region *J. Appl. Spectrosc.* **10** 656–7

[17] Jewell J M 1991 Thermooptic coefficients of some standard reference material glasses *J. Am. Ceram. Soc.* **74** 1689–91

[18] Arndt J and Stöffler D 1969 Anomalous changes in some properties of silica glass densified at very high pressures *Phys. Chem. Glasses* **10** 117–24

[19] Fujino S, Takebe H and Morinaga K 1995 Measurements of refractive indexes and factors affecting dispersion in oxide glasses *J. Am. Ceram. Soc.* **78** 1179–84

[20] Vedam K, Schmidt E D D and Roy R 1966 Nonlinear variation of refractive index of vitreous silica with pressure to 7 Kbars *J. Am. Ceram. Soc.* **49** 531–5

[21] Cohen H M and Roy R 1965 Densification of glass at very high pressures *Phys. Chem. Glasses* **6** 149–61

[22] Cohen H M and Roy R 1961 Effects of ultra high pressures on glass *J. Am. Ceram. Soc.* **44** 523–4

[23] Malitson I H 1965 Interspecimen comparison of the refractive index of fused silica *J. Opt. Soc. Am.* **55** 1205–9

[24] Brixner B 1967 Refractive-index interpolation for fused silica *J. Opt. Soc. Am.* **57** 674–6

[25] Matsuoka J, Kitamura N, Fujinaga S, Kitaoka T and Yamashita H 1991 Temperature dependence of refractive index of SiO_2 glass *J. Non-Cryst. Solids* **135** 86–9

[26] Waxler R M and Cleek G W 1971 Refractive indices of fused silica at low temperatures *J. Res. Natl Bur. Stand.* A **75A** 279–81

[27] Yamamuro T *et al* 2006 Measurement of refractive indices of 20 optical materials at low temperatures *Opt. Eng.* **45** 083401

[28] Rodney W S and Spindler R J 1954 Index of refraction of fused quartz glass for ultraviolet, visible, and infrared wavelengths *J. Opt. Soc. Am.* **44** 677–9

[29] Vannoni M, Olivieri M, Mondello G, Sordini A and Molesini G 2010 Refractive index of Lithosil and Suprasil 312 at cryogenic temperature *Metrologia* **47** 175

[30] Born M and Wolf E 2013 *Principles of Optics: Electromagnetic Theory of Propagation, Interference and Diffraction of Light* (Amsterdam: Elsevier)

[31] Vishnyakov G N, Levin G G, Kornysheva S V, Zyuzev G N, Lyudomirskii M B, Pavlov P A and Filatov Y V 2005 Measuring the refractive index on a goniometer in the dynamic regime *J. Opt. Technol.* **72** 929–34

[32] Kuiper M, Koops R, Nieuwland R and van der Pol E 2022 Software Underlying 'Method to Traceably Determine the Refractive Index by Measuring the Angle of Minimum Deviation' *Zenodo* https://doi.org/10.5281/zenodo.5801199

[33] Bönsch G and Potulski E 1998 Measurement of the refractive index of air and comparison with modified Edlén's formulae *Metrologia* **35** 133

[34] Sansonetti C J, Salit M L and Reader J 1996 Wavelengths of spectral lines in mercury pencil lamps *Appl. Opt.* **35** 74–7

[35] International Organization for Standardization 2008 *Uncertainty of Measurement: III. Guide to the Expression of Uncertainty in Measurement (GUM:1995)—Supplement 1: Propagation of Distributions Using a Monte Carlo Method*

[36] de Rond L, Coumans F A W, Nieuwland R, van Leeuwen T G and van der Pol E 2018 Deriving extracellular vesicle size from scatter intensities measured by flow cytometry *Curr. Protoc. Cytom.* **86** e43